Chiral edge currents for ac-driven skyrmions in confined pinning geometries

C. Reichhardt and C. J. O. Reichhardt

Theoretical Division and Center for Nonlinear Studies, Los Alamos National Laboratory, Los Alamos, New Mexico 87545, USA

We show that ac-driven skyrmion lattices in a weak pinning channel confined by regions of strong pinning exhibit edge transport carried by skipping orbits while skyrmions in the bulk of the channel undergo localized orbits with no net transport. The magnitude of the edge currents can be controlled by varying the amplitude and frequency of the ac drive or by changing the ratio of the Magnus force to the damping term. We identify a localized phase in which the orbits are small and edge transport is absent, an edge transport regime, and a fluctuating regime that appears when the ac drive is strong enough to dynamically disorder the skyrmion lattice. We also find that in some cases, multiple rows of skyrmions participate in the transport due to a drag effect from the skyrmion-skyrmion interactions. The edge currents are robust for finite disorder and should be a general feature of skyrmions interacting with confined geometries or inhomogeneous disorder under an ac drive. We show that similar effects can occur for skyrmion lattices at interfaces or along domain boundaries for multiple coexisting skyrmion species. The edge current effect provides a new method to control skyrmion motion, and we discuss the connection of these results with recent studies on the emergence of edge currents in chiral active matter systems and gyroscopic metamaterials.

I. INTRODUCTION

A paradigmatic example of a system that exhibits edge states or edge currents in confinement is electrons in a magnetic field undergoing cyclotron motion. Here, bulk electrons follow closed circular orbits while charges near the boundaries enter skipping orbits, and the direction of the resulting current is determined by the chirality of the cyclotron motion [1–5]. Edge currents also arise in cold atom systems [6], chiral active matter spinners [7–10], coupled gyroscopes [11–14], and colloids placed on periodic magnetic substrates to create colloidal topological insulators [15,16] in analogy to electronic topological insulators [17]. In all of these systems, there is some form of periodic orbit with a particular chirality as well as some type of boundary or interface. Edge currents can also arise for magnetic skyrmions, which have dynamics that are similar in many ways to those of electrons in a magnetic field. Skyrmions can exhibit complex cyclotron orbits with a fixed chirality, and in certain sample geometries, the skyrmions interact with some form of boundary or interface [18,19].

Skyrmions are particlelike textures that were originally proposed to appear in magnets in 1989 [20]. Magnetic skyrmion lattices were experimentally observed in 2009 using neutron scattering [21] and were directly imaged with Lorentz microscopy [22]. Since these initial observations, an increasing variety of materials have been identified which support skyrmions, including systems in which skyrmions are stable at room temperature [23–27]. When skyrmions are set into motion by an applied current [28–34], they exhibit depinning and sliding phases similar to those found for vortices in type-II superconductors and Wigner crystals [35]. Due to their size scale and the fact that they can be moved easily with a current, skyrmions are also candidates for possible memory and computing applications [36–39], and

the understanding of skyrmion dynamics on the individual and collective level will be integral to the creation of such devices. Although skyrmions have many similarities to other particle-based systems that exhibit depinning, they also have several distinct properties, the most prominent of which is the domination of skyrmion dynamics by the Magnus force. Skyrmion motion has features that resemble the dynamics of electrons in a magnetic field; however, the skyrmions can also experience significant damping, and the ratio of the Magnus force to the damping force depends on the material parameters and can produce different dynamical effects [18,19,27,28,40]. The Magnus force generates a skyrmion velocity component that is perpendicular to the net external force acting on the skyrmion. One consequence of a finite Magnus term is that the skyrmions move at an angle with respect to an applied drive that is known as the skyrmion Hall angle [18,19,21]. In the absence of quenched disorder or pinning, the skyrmion Hall angle is constant; however, when quenched disorder is present, the skyrmion Hall angle becomes drive or velocity dependent, starting at a value of nearly zero just above the depinning threshold and approaching the disorder-free limit at higher drives [41–48]. The Magnus force also causes the skyrmions to exhibit cyclotron or spiraling motion when they are in a confining potential or interacting with a pinning site [41,49–56]. Skyrmions can perform circular orbits under biharmonic drives [57], oscillating fields [58,59], and in certain types of driven bilayer systems [60]. In numerical studies of skyrmions with one-dimensional (1D) periodic and asymmetric substrate arrays, skyrmions under ac, dc, and combined ac and dc drives exhibited complex periodic closed and running orbits [61–63].

Since skyrmions can undergo chiral motion when interacting with disorder or subjected to a drive, it is natural to look for edge currents in the presence of a confining

geometry when the skyrmions are driven or perturbed in some way. In this paper, we examine skyrmion lattices in a system containing a pin-free channel surrounded by strong pinning, with an initially uniform distribution of skyrmions in the entire sample. Under an ac drive, the skyrmions in the pin-free channel undergo periodic motion. If there were no confinement, the periodic orbits would take the form of 1D paths oriented at an angle to the applied drive; however, when confinement is present, the skyrmions near the edges of the pin-free channel follow circular or elliptical orbits with a chirality that is determined by the sign of the Magnus force. These orbits interact with the edge potential created by the pinned skyrmions and become skipping orbits that generate edge currents moving to the right or left, depending on the side of the pin-free channel at which they appear. The skyrmions in the bulk of the pin-free channel remain localized. We find slip phenomena for the skyrmions participating in the edge transport, and the effectiveness of the edge currents depends on the ratio of the Magnus force to the damping force as well as on the amplitude and frequency of the ac drive and on the skyrmion density.

We identify three regimes of behavior. For ac drives with high frequency or low amplitude, we observe a localized phase in which no edge transport occurs but the orbits at the edges of the pin-free channel are much more circular than the orbits in the bulk of the pin-free channel. We also find a regime of edge transport in which the skyrmions in the pin-free channel form a lattice, as well as a liquid regime in which the ac drive is large enough to melt the skyrmion lattice dynamically. Within the liquid regime, near the transition to the lattice regime, edge transport can still appear in which skyrmions at the edge of the pin-free channel can be transported over some distance before exchanging with skyrmions in the bulk of the pin-free channel; however, deeper within the liquid regime, the edge transport is lost. In the limit of zero Magnus force, there is no edge transport and the orbits are 1D throughout the sample. The edge transport we observe is a collective effect, and it does not appear in the low density limit.

We also find that the width and type of orbit along the edge of the pin-free channel depend on the direction of the applied ac drive. When the drive is parallel to the channel, pronounced edge transport appears, while a drive that is perpendicular to the channel generally produces less edge transport since the orbits become 1D and are oriented parallel to the edge of the channel. In regimes where strong edge transport occurs, the moving skyrmions along the edge can drag the adjacent rows of skyrmions, causing these rows to exhibit a drift of reduced magnitude. These effects are robust for varying amounts of disorder, and in some cases, a disorder-free system that shows no edge transport can develop edge currents when disorder is introduced. In the low-density regime, the edge transport is generally weak or absent, but we find that commensurate-incommensurate effects between 1D rows of skyrmions can create currents flowing in the bulk of the pin-free channel instead of along its edges. Such effects occur when the edge row and an adjacent row contain different numbers of skyrmions, producing a skyrmion gear motion. Finally, we show that edge currents should be a general feature that appears at any type of skyrmion interface, such as along the domain wall separating two different species of skyrmions. These effects should arise

for confining geometries under ac drives in samples with inhomogeneous pinning, edge roughness, grain boundaries, or twin boundaries. Our results provide a new method for transporting skyrmions that avoids the skyrmion Hall effect found for dc-driven skyrmions.

The paper is organized as follows. In Sec. II, we discuss the system and the simulation method. In Sec. III, we describe the conditions under which edge currents arise and demonstrate the different dynamical regimes. Section IV shows the effect of applying the ac driving along different directions, while in Sec. V, we examine the role of disorder. In Section VI, we vary the skyrmion density and explore skyrmion pumping produced by commensurate-incommensurate effects, while in Sec. VII, we discuss our results, describe geometries in which the edge currents could arise, and show that edge currents can occur even for pin-free systems at an interface between different skyrmion species. In Sec. VIII, we summarize our results.

II. SIMULATION

We consider a two-dimensional (2D) system of size $L \times L$ with periodic boundary conditions in the x and y directions. Half of the sample contains a square array of pinning sites, and the other half of the sample consists of a pin-free channel aligned with the x direction. The system contains N_{sk} skyrmions and N_p pinning sites. The skyrmion density is $n_{sk} = N_{sk}/L^2$ and the matching density at which the number of skyrmions would equal the number of pins in a sample with uniform pinning is $n_\phi = 2N_p/L^2$. The initial positions of the skyrmions are obtained using simulated annealing. The skyrmion-skyrmion interactions are repulsive, and in the absence of pinning, the skyrmions form a uniform triangular lattice. After annealing, we apply an ac drive parallel or perpendicular to the pin-free channel.

In Fig. 1(a), we illustrate the skyrmion locations and trajectories in a pin-free system under an ac drive applied along the x direction. Here the skyrmions form a triangular lattice and execute 1D orbits oriented at an angle with respect to the drive direction given by the skyrmion Hall angle θ_{sk}^{int}. In Fig. 1(b), half of the sample contains a square pinning lattice and a pin-free channel is oriented along the x direction. Here, when an ac drive is applied, the skyrmions in the pinning sites remain immobile and produce a confining potential for the skyrmions in the pin-free channel. Within the pin-free channel, the skyrmions form a triangular lattice but no longer undergo the strictly 1D motion of Fig. 1(a). Instead, the skyrmions follow circular or elliptical orbits, with a continuously translating or edge current appearing along the edges of the channel, as highlighted by the arrows. The skyrmions in the bulk of the pin-free channel perform localized orbits. In this case, the skyrmion orbits are counterclockwise, so the skyrmions on the bottom edge of the pin-free channel are moving in the $-x$ direction while those on the top edge of the channel are translating in the $+x$ direction.

We model the skyrmions using a particle based approach for skyrmions interacting with pinning as employed previously [40,41,61–64]. The motion of skyrmion i is governed by the following equation of motion:

$$\alpha_d \mathbf{v}_i + \alpha_m \hat{z} \times \mathbf{v}_i = \mathbf{F}_i^{ss} + \mathbf{F}_i^{sp} + \mathbf{F}_i^{ac}. \tag{1}$$
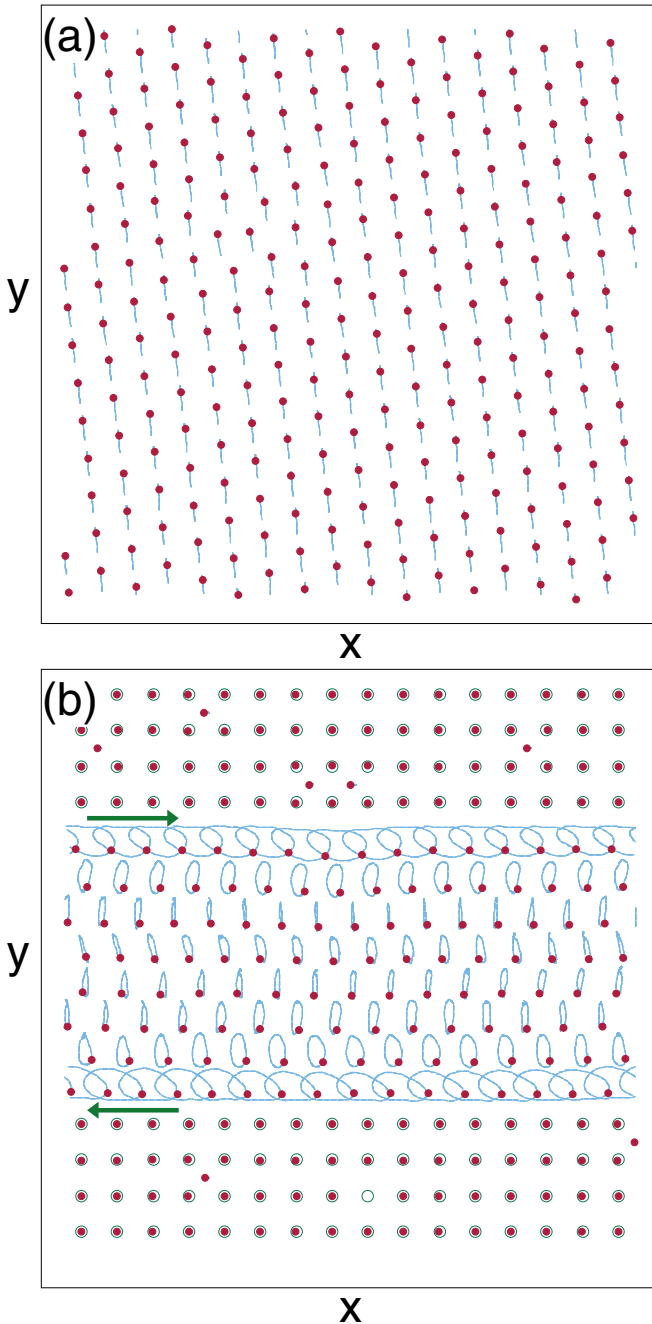
FIG. 1. (a) Skyrmion positions (dots) and trajectories (lines) for a system without any pinning at a skyrmion density of $n_{sk} = 0.2$ and a matching density of $n_\phi = 0.2$ for $\alpha_m/\alpha_d = 10.0$ under an x-direction ac drive with amplitude $A = 0.075$ and frequency $\omega = 3.75 \times 10^{-5}$. The skyrmions form a triangular lattice and move at an angle of $\theta = 84°$ with respect to the driving direction. (b) The same for a sample in which half of the system is filled with a square array of pinning sites (open circles). The skyrmions in the pin-free channel form a triangular lattice and execute closed counterclockwise orbits, while the skyrmions in the pinned region remain immobile. Edge transport occurs along the boundaries of the pin-free channel, as indicated by the arrows.

Force is measured in units of J_{ex}/d, where J_{ex} is the exchange energy and d is the thickness of the sample, and distance is measured in units of J_{ex}/D, where D is the strength of

the Dzyaloshinskii-Moriya interaction. The first term on the right is the repulsive skyrmion-skyrmion interaction force $\mathbf{F}_i = \sum_{j\neq i}^N K_1(r_{ij})\hat{\mathbf{r}}_{ij}$, where $r_{ij} = |\mathbf{r}_i - \mathbf{r}_j|$ is the distance between skyrmions i and j and $K_1(r)$ is the modified Bessel function which decreases exponentially at large r. The pinning force is given by $\mathbf{F}_i^{sp}$ and the pinning sites are modeled as parabolic traps of maximum strength F_p and radius r_p. In this work, we set F_p sufficiently large that skyrmions within the pinning sites remain immobile for all the parameters we consider. Additionally, r_p is small enough that each pinning site captures at most one skyrmion. We focus on the regime in which there are twice as many skyrmions as pinning sites, so that the pin-free and pinned regions contain equal numbers of skyrmions. Our model does not include internal modes of the skyrmions, which could modify the skyrmion motion. Provided that the skyrmions remain reasonably well separated and are not subjected to very large currents that could excite the internal modes, we expect the behavior we find here to be generic to skyrmion systems.

An ac driving force $\mathbf{F}^{ac}$ is applied in either the x or y direction, $\mathbf{F}^{ac} = A\sin(\omega t)(\hat{\mathbf{x}}, \hat{\mathbf{y}})$. The term α_d is the damping constant which aligns the velocities in the direction of the net force while α_m is the coefficient of the Magnus term which aligns the velocity perpendicular to the net force. The dynamics can be characterized by the ratio α_m/α_d, and in the absence of pinning the skyrmions move at an angle with respect to a dc drive known the intrinsic skyrmion Hall angle $\theta_{sk}^{int} = \arctan(\alpha_m/\alpha_d)$. When $\alpha_m = 0$, the system is in the overdamped limit. The initial positions of the skyrmions are obtained by starting from a high temperature liquid state and cooling to $T = 0.0$ in order to obtain an overall skyrmion density that is roughly constant in both the pinned and unpinned regions.

III. EDGE TRANSPORT AND DYNAMICAL REGIMES

A. Edge transport

We first illustrate that skyrmions translate along the edges of the pin-free region. In Fig. 2, we plot the x position versus ac cycle number n for individual skyrmions on the bottom edge, top edge, and center of the pin-free channel in a system with $\alpha_m/\alpha_d = 15$, $n_{sk} = 0.4$, $n_\phi = 0.4$, $A = 0.075$, and $\omega = 3.75 \times 10^{-5}$. All three skyrmions start at an x position near $x = 29$. In Fig. 3(a), we illustrate the skyrmion positions, pinning site locations, and trajectories for all skyrmions from the system in Fig. 2, while in Fig. 3(b), we trace the trajectories of only the three skyrmions shown in Fig. 2. The skyrmion on the bottom edge of the pin-free channel moves in the $-x$ direction, undergoing a displacement of $\delta x = -45$ during the course of 70 ac cycles, as shown in Fig. 2. The skyrmion on the top edge of the pin-free channel moves a distance of $\delta x = 30$ in the positive x direction during the same time period, and the skyrmion at the center of the channel has no net displacement. The skyrmions that are undergoing a net translation do not exhibit completely periodic motion but occasionally become localized for a period of time when phase slips occur, producing the disorder in the orbits found in Fig. 3(b). Since the lattice constant of the pinning sites is $a = 1.56$, if the skyrmion lattice was perfectly ordered and the
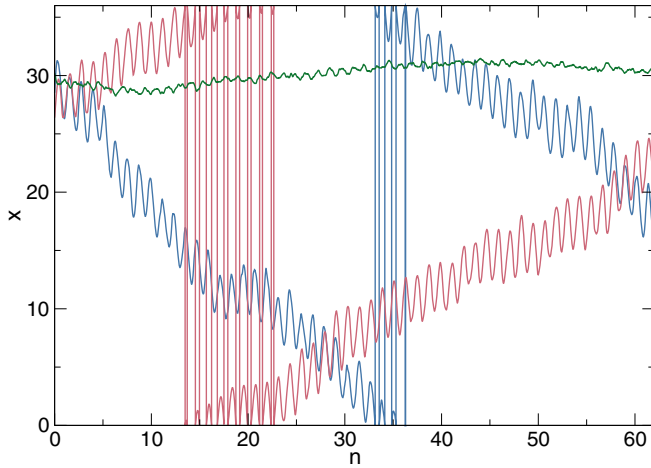
FIG. 2. x position vs ac cycle number n for individual skyrmions at the bottom edge of the pin-free channel (blue), the top edge of the pin-free channel (red), and in the center of the pin-free channel (green) in a sample with x direction driving, $\alpha_m/\alpha_d = 10$, $A = 0.075$, $\omega = 3.75 \times 10^{-5}$, skyrmion density $n_{sk} = 0.4$, and matching density $n_\phi = 0.4$. The skyrmion on the top edge moves in the positive x direction, the skyrmion on the bottom edge moves in the negative x direction, and the skyrmion in the center remains localized. The trajectories of these three skyrmions are illustrated in Fig. 3(b). The jumps between $x = 0$ and $x = 36$ occur when the skyrmion crosses the periodic boundary.

skyrmion orbit perfectly matched the pinning lattice size scale to produce an ideal locking between the cyclic orbit and the periodic drive, a total displacement of $|\delta x_{ideal}| = 110$ would occur during the course of $n = 70$ cycles. The size of the elliptical orbit on the edges of the pin-free channel depends on the frequency and amplitude of the ac drive as well as on the value of α_m/α_d, so the efficiency $|\delta x|/|\delta x_{ideal}|$ of the transport current depends on these parameters.

The edge current results from a ratchet mechanism, in which ac driving is converted to a dc drift [65]. Ratchets exist only in nonequilibrium systems, and they require that a sufficient number of symmetries be broken. Here, temporal symmetry is broken by the ac drive and spatial symmetry is broken by the edges of the channel. Other examples of ratchet effects include systems in which the substrate is spatially symmetric but temporal symmetry is broken by two superimposed ac drives [66–69], as well as systems in which both spatial and temporal symmetry is broken [70–72].

B. Varied A and ω

We next show that three dynamical regimes emerge as we vary the ac drive amplitude A and frequency ω. In Fig. 4, we plot the skyrmion trajectories for the system from Fig. 3 at different values of A and ω. Figures 4(a) and 4(b) show systems with $A = 0.075$ at higher frequencies of $\omega = 6 \times 10^{-5}$ and $\omega = 1 \times 10^{-4}$, respectively. Edge currents are still present when $\omega = 6 \times 10^{-5}$ in Fig. 4(a), but in Fig. 4(b) at $\omega = 1 \times 10^{-4}$, the edge transport is lost, with skyrmions at the edge of the pin-free channel executing circular orbits and skyrmions in the bulk of the pin-free channel following 1D trajectories. In general, as the ac drive frequency increases,
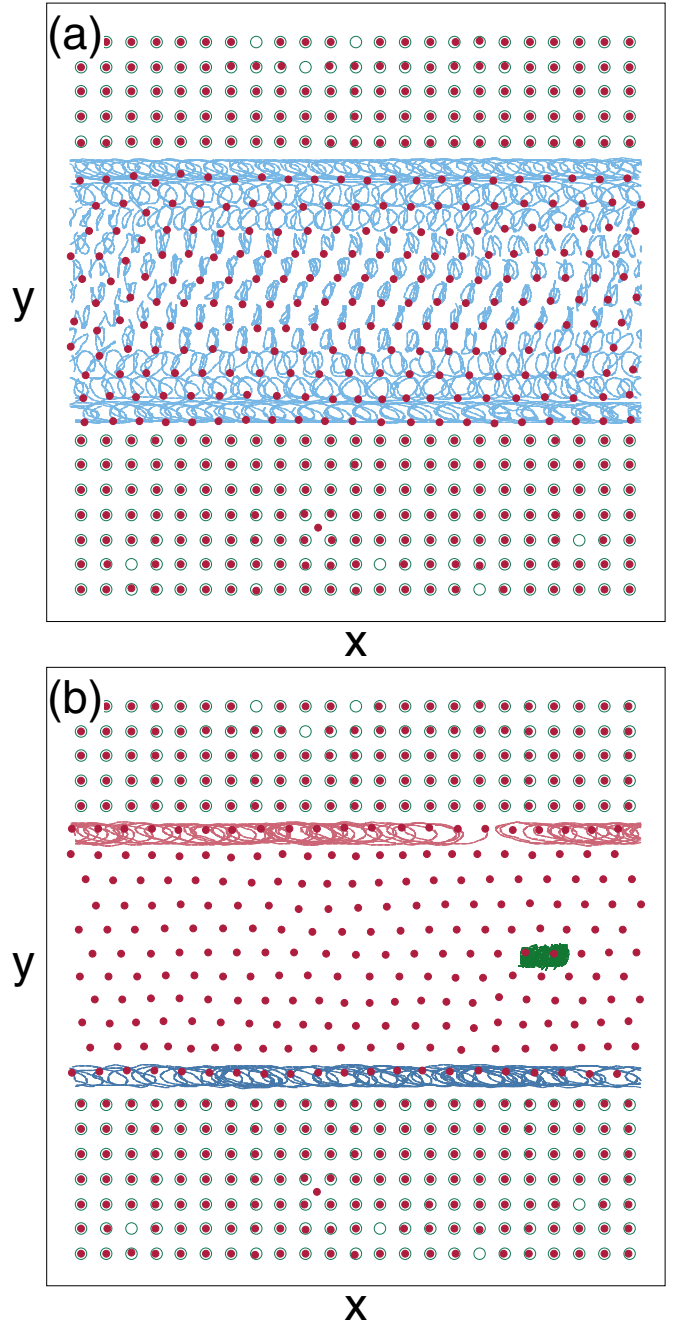

FIG. 3. Skyrmion positions (dots), all skyrmion trajectories (lines), and pinning site locations (open circles) for the system in Fig. 2 with x direction ac driving illustrating the edge transport. Here, $\alpha_m/\alpha_d = 10$, $A = 0.075$, $\omega = 3.75 \times 10^{-5}$, and $n_{sk} = n_\phi = 0.4$. (b) Image of the same system with the trajectories of only the three skyrmions shown in Fig. 2 plotted. Red: Skyrmion at the top of pin-free channel; green: Skyrmion in the center of pin-free channel; blue: Skyrmion at the bottom of the pin-free channel.

the size of the skyrmion orbits shrinks, but edge transport only occurs when the orbits are large enough that they either overlap with each other or are wider than the period of the confining potential. Figure 4(c) shows a sample with $\omega = 3.75 \times 10^{-5}$ at a smaller $A = 0.025$, where the orbits are small enough that the edge currents are lost. In Fig. 4(d) at
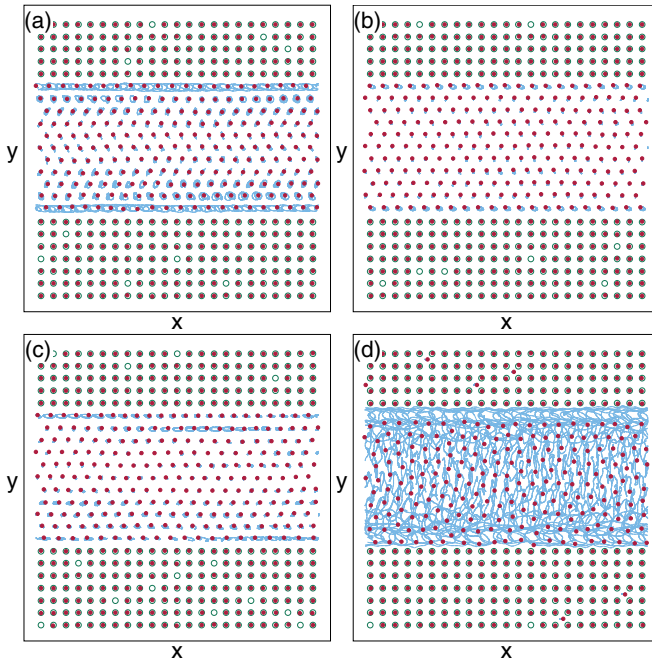
FIG. 4. Skyrmion positions (dots), trajectories (lines), and pinning site locations (open circles) for the system in Fig. 2 at different x direction ac drive frequencies and amplitudes, where $\alpha_m/\alpha_d = 10$ and $n_{sk} = n_\phi = 0.4$. (a) In the edge transport phase at $\omega = 6 \times 10^{-5}$ and $A = 0.075$, the orbits are smaller but edge transport persists. (b) In the localized lattice phase at $\omega = 1 \times 10^{-4}$ and $A = 0.075$, the orbits are small enough that no edge transport occurs. (c) In the localized lattice phase at $\omega = 3.75 \times 10^{-5}$ and $A = 0.025$, there is also no edge transport due to the small size of the orbits. (d) The disordered or fluctuating phase at $\omega = 3.75 \times 10^{-5}$ and $A = 0.15$.

$\omega = 3.75 \times 10^{-5}$ and $A = 0.15$, the orbits are large enough that the skyrmions in the pin-free channel become strongly disordered and form a dynamical liquid or fluctuating state. In this fluctuating regime, it is still possible for edge transport to occur when skyrmions near the edges of the channel translate for some distance before exchanging with a skyrmion in the bulk of the pin-free channel. Thus, we observe both a crystal with edge transport and a liquid with edge transport. For larger values of A, the skyrmions become more disordered and the edge transport is strongly reduced or absent, and when A is sufficiently large, the skyrmions at the pinning sites begin to depin and the distinction between skyrmions in the pin-free channel and those in the pinned region is destroyed.

In Fig. 5, we plot the average drift distance $\langle d \rangle = N_{edge}^{-1} \sum_{i=1}^{N_{edge}} |\delta x_i|$ for the N_{edge} skyrmions on the edges of the pin-free channel during a time period of $n = 20$ ac drive cycles. Figures 5(a) and 5(b) shows $\langle d \rangle$ versus A and ω, respectively, for the system in Fig. 4 at $\alpha_m/\alpha_d = 15$. In both cases there is an optimum drive parameter that maximizes the edge transport, while for low A or high ω, the edge skyrmions are localized. In Fig. 5(a), when $A > 0.115$ the skyrmion lattice starts to become disordered and forms a liquid state. Figure 5(b) indicates that the edge transport is more efficient at lower frequencies since fewer phase slips occur; however, the orbits also become increasingly one-dimensional as ω decreases, so at small values of ω the edge transport is reduced.
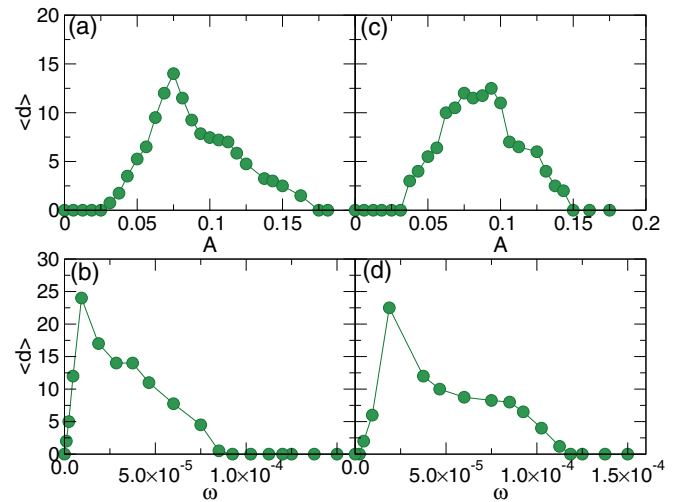

FIG. 5. The average drift distance $\langle d \rangle$ for the edge skyrmions during 20 ac drive cycles for the system in Fig. 4(a) with x direction driving and $n_{sk} = n_\phi = 0.4$. (a) $\langle d \rangle$ vs A for a sample with $\alpha_m/\alpha_d = 15$ at $\omega = 3.75 \times 10^{-5}$. (b) $\langle d \rangle$ vs ω for the system in (a) at $A = 0.075$. (c) $\langle d \rangle$ vs A for a sample with $\alpha_m/\alpha_d = 5.0$ at $\omega = 3.75 \times 10^{-5}$. (d) $\langle d \rangle$ vs ω for the system in (c) at $A = 0.075$.

In Figs. 5(c) and 5(d), we plot $\langle d \rangle$ versus A and ω for a system with $\alpha_m/\alpha_d = 5.0$, where similar behavior appears.

C. Varied α_m/α_d

We find the same three phases when we vary the ratio α_m/α_d of the Magnus force to the damping term. In Fig. 6, we illustrate the skyrmion trajectories for varied α_m/α_d. In the overdamped limit of $\alpha_m/\alpha_d = 0.0$, shown in Fig. 6(a) for $A = 0.075$ and $\omega = 3.75 \times 10^{-5}$, there are no edge currents and the skyrmions in the pin-free channel move in strictly 1D paths aligned with the x-direction. Here the orbits are large enough that they overlap. In Fig. 6(b), the orbits for a system with $\alpha_m/\alpha_d = 0.5$, $A = 0.025$, and $\omega = 1.5 \times 10^{-4}$ are elliptical but there are still no edge currents. The sample with $\alpha_m/\alpha_d = 5.0$, $A = 0.075$, and $\omega = 3.75 \times 10^{-5}$ illustrated in Fig. 6(c) has strong edge transport as well as transport of skyrmions that are up to three rows from the edge of the pin-free channel. This occurs when the edge transport is sufficiently strong that it exerts a drag effect on the adjacent rows, which pick up a net motion at a reduced velocity. In Fig. 7, we illustrate the x position of individual skyrmions in the top, second from top, and third from top rows in the pin-free channel for the system in Fig. 6(c). Each of these rows has a net transport in the positive x direction, but the magnitude of the transport decreases as the rows become further from the edge of the channel. The forth row from the top of the channel has no net drift. Similarly, at the bottom of the pin-free channel (not shown) the three rows closest to the channel edge are moving in the $-x$ direction. We have also found regimes in which only two rows are moving as well as regimes in which only the edgemost row is moving. Figure 6(d) shows the skyrmion trajectories for a sample with $\alpha_m/\alpha_d = 25$, $\omega = 3.75 \times 10^{-5}$, and $A = 0.075$. The orbits are smaller than those that appear for the same ac drive parameters
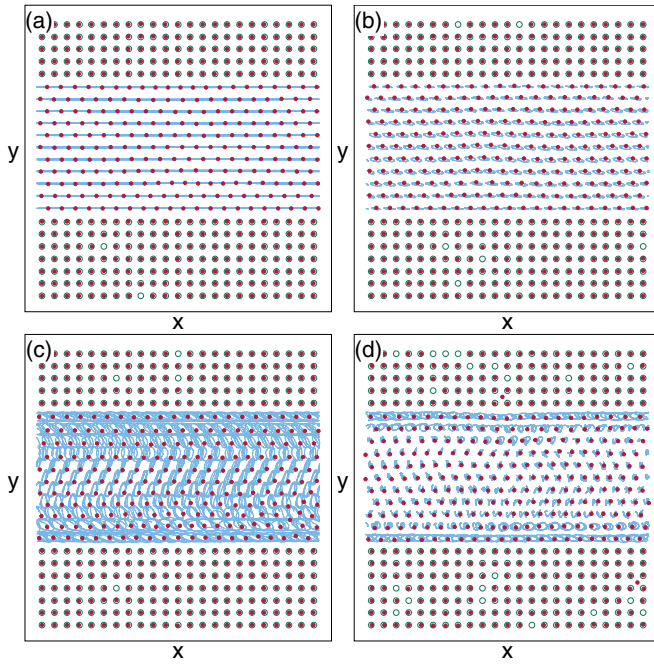
FIG. 6. Skyrmion positions (dots), trajectories (lines), and pinning site locations (open circles) for varied ratios of the Magnus force to the damping term in samples with x direction driving and $n_{sk} = n_\phi = 0.4$. (a) In the overdamped $\alpha_m/\alpha_d = 0.0$ limit at $A = 0.075$ and $\omega = 3.75 \times 10^{-5}$, there is no edge transport and the skyrmions move in strictly 1D orbits. (b) In the localized lattice phase at $A = 0.025$ and $\omega = 1.5 \times 10^{-4}$ for $\alpha_m/\alpha_d = 0.5$, there is no edge transport and the skyrmions move in elliptical paths. (c) In the edge transport phase at $A = 0.075$ and $\omega = 3.75 \times 10^{-5}$ for $\alpha_m/\alpha_d = 5$, there are multiple rows participating in the edge transport. (d) In the edge transport phase at $A = 0.075$ and $\omega = 3.75 \times 10^{-5}$ for $\alpha_m/\alpha_d = 20$, the edge transport involves only the edgemost rows and the skyrmion orbits are smaller.
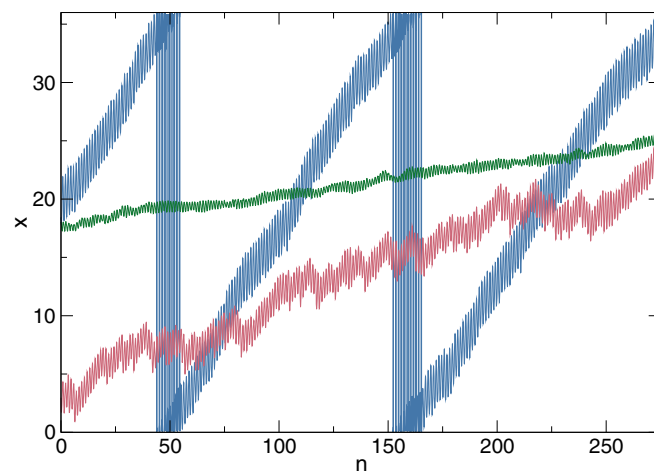

FIG. 7. x position vs ac cycle number n for individual skyrmions in the first (blue), second (red), and third (green) rows from the top of the pin-free channel for the sample in Fig. 6(c) with x direction driving in an edge transport phase at $n_{sk} = n_\phi = 0.4$, $\alpha_m/\alpha_d = 5.0$, $\omega = 3.75 \times 10^{-5}$, and $A = 0.075$. Multiple rows are moving but the transport is reduced for rows that are further from the edge of the pin-free channel.
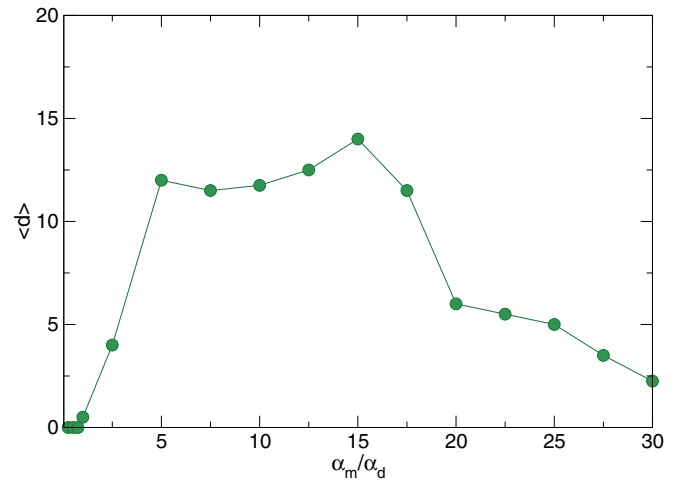

FIG. 8. $\langle d \rangle$ vs α_m/α_d for an x direction ac drive with $\omega = 3.75 \times 10^{-5}$ and $A = 0.075$, showing that $\langle d \rangle$ goes to zero in the overdamped limit of $\alpha_m/\alpha_d = 0.0$. Here $n_{sk} = n_\phi = 0.4$.

at $\alpha_m/\alpha_d = 15$ or 10 since the skyrmion orbits become more curved when the Magnus force is larger. When the skyrmion orbits are smaller, the edge currents are reduced in magnitude.

In Fig. 8, we plot $\langle d \rangle$ versus α_m/α_d for an ac drive with $\omega = 3.75 \times 10^{-5}$ and $A = 0.075$. Edge currents are absent when α_m/α_d is small. For $2.5 < \alpha_m/\alpha_d < 17.5$, multiple rows participate in the edge transport, while for $\alpha_m/\alpha_d \geqslant 17.5$, only the outer row of the pin-free channel has a net transport. The overall shape of $\langle d \rangle$ versus α_m/α_d depends strongly on the values of ω and A, and if these quantities are too small, $\langle d \rangle = 0.0$.

By varying A, ω, and α_m/α_d, we identify three regimes of behavior: A localized lattice phase with no edge transport, an edge transport phase in which the skyrmions remain in a lattice structure, and a disordered or fluctuating state. In Fig. 9, we construct a dynamic phase diagram as a function
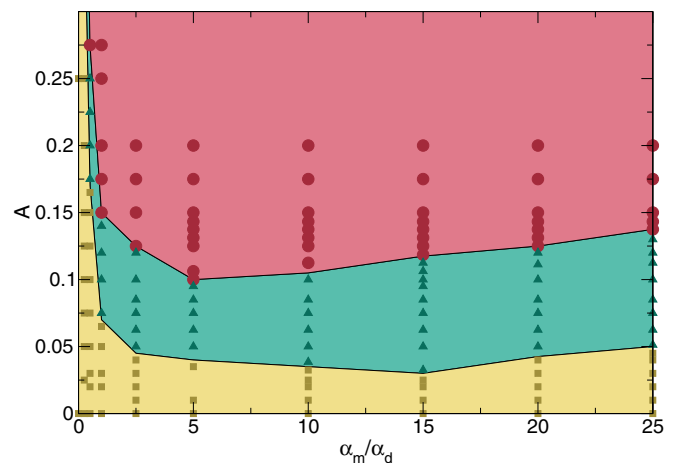

FIG. 9. Dynamic phase diagram as a function of A vs α_m/α_d for fixed $\omega = 3.75 \times 10^{-5}$ and x direction driving in samples with $n_{sk} = n_\phi = 0.4$. Squares (yellow): Localized state; triangles (green): Crystal state with edge currents; circles (red): Disordered fluctuating state.

of A versus α_m/α_d for a system with fixed $\omega = 3.75 \times 10^{-5}$, highlighting the localized phase, lattice edge transport phase, and fluctuating liquid phase. As α_m/α_d approaches zero, the localized phase grows in extent. In the overdamped limit, the skyrmions form a triangular lattice that moves elastically back and forth in the x direction with no net transport, as illustrated in Fig. 6(a). Figure 9 indicates that there is a tendency for the localized region to grow at large values of α_m/α_d due to the shrinking of the skyrmion orbit size with increasing Magnus force. Within the fluctuating regime, there is still some transport of skyrmions along the edges at smaller values of A; however, for larger A the system becomes more liquidlike and the edge transport vanishes. We can construct a similar phase diagram for fixed A and varied ω (not shown), where we find that at high drive frequencies, the system enters the localized regime.

IV. AC DRIVING IN THE PERPENDICULAR DIRECTION

Up until now we have considered a driving force applied along the x direction, parallel to the pin-free channel. In this orientation, the Magnus force generated by the drive produces a skyrmion velocity component aligned mostly along the y di-
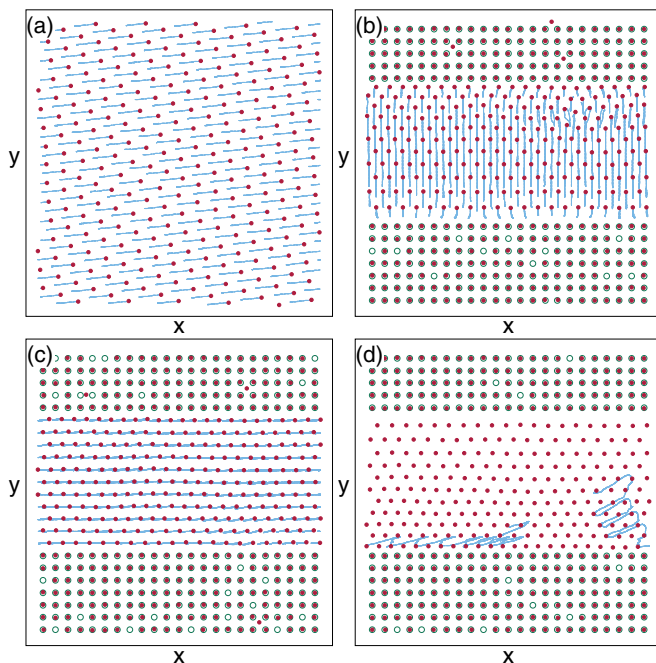
FIG. 10. Skyrmion positions (dots), trajectories (lines), and pinning site locations (open circles) for systems with $n_{sk} = n_\phi = 0.4$ in which the ac drive is applied in the y direction. (a) A sample with no pinning at $A = 0.075$, $\omega = 3.75 \times 10^{-5}$, and $\alpha_m/\alpha_d = 10$. The trajectories are 1D in nature and are aligned mostly along the x direction. (b) The same sample with pinning at $\alpha_m/\alpha_d = 0.0$ in the localized lattice phase for $A = 0.075$ and $\omega = 3.75 \times 10^{-5}$, where there are no edge currents. (c) In the edge transport phase at $\alpha_m/\alpha_d = 10.0$ for $A = 0.075$ and $\omega = 3.75 \times 10^{-5}$, edge currents appear. (d) The fluctuating state at $\alpha_m/\alpha_d = 2.0$, $A = 0.075$, and $\omega = 5 \times 10^{-6}$ where the trajectory of only a single skyrmion is plotted. This skyrmion undergoes edge transport before becoming trapped in the bulk of the pin-free channel.
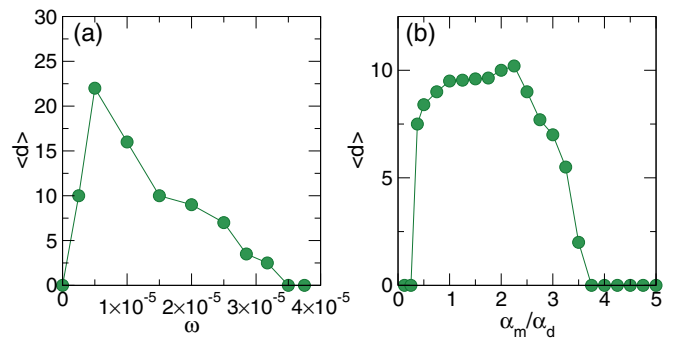
FIG. 11. (a) $\langle d \rangle$ vs ω at $\alpha_m/\alpha_d = 2$ and (b) $\langle d \rangle$ vs α_m/α_d at $\omega = 5 \times 10^{-6}$ for the system in Fig. 10(d) with y direction driving, $n_{sk} = n_\phi = 0.4$, and $A = 0.075$.

rection. If the ac drive is instead applied along the y direction, perpendicular to the pin-free channel, the Magnus-induced velocity is mostly aligned with the x direction, and as a result, for large α_m/α_d, the skyrmion trajectories become nearly 1D along the x direction and the edge currents are absent.

In Fig. 10(a), we illustrate the skyrmion trajectories in the absence of pinning for a system with an ac drive applied along the y direction at $A = 0.075$, $\omega = 3.75 \times 10^{-5}$, and $\alpha_m/\alpha_d = 10$. Here the skyrmions follow 1D paths that are aligned mostly in the x-direction. Figure 10(b) shows the same system with pinning present in the overdamped limit of $\alpha_m/\alpha_d = 0.0$. The skyrmions in the pin-free channel move in 1D paths aligned in the y direction and there is no edge transport. In Fig. 10(c) at $\alpha_m/\alpha_d = 10$, the skyrmions move in mostly 1D paths aligned with the x direction, and edge transport is absent. In general, for driving in the y direction, we only observe edge transport for low values of α_m/α_d and low ac drive frequencies ω. The edge transport is the most efficient when the system is near the transition to the fluctuating state. In Fig. 10(d) at $A = 0.075$, $\alpha_m/\alpha_d = 2.0$, and $\omega = 5 \times 10^{-6}$, just past the transition to the fluctuating state, we highlight the trajectory of a single skyrmion that undergoes edge transport when it is near the edge of the pin-free channel. The skyrmion eventually wanders off into the bulk and becomes trapped.

In Fig. 11(a) and 11(b), we plot $\langle d \rangle$ versus ω and $\langle d \rangle$ versus α_m/α_d, respectively, for the system in Fig. 10(d). The frequency and amplitude dependence of the edge currents is similar to that found for driving in the x direction. Here there are no edge currents for $\alpha_m/\alpha_d > 3.5$ since the orbits become too one-dimensional.

V. EFFECTS OF DISORDER

We next consider the addition of disorder, achieved by applying random offsets to the pinning site locations in both the x and y directions. The offsets are uniformly distributed and have a maximum size of δr, which is always less than $0.5a$, where a is the pinning lattice constant. Depending on the parameters, we find that the disorder can enhance or decrease the edge transport. In Fig. 12(a), we illustrate the skyrmion positions and trajectories for a system with $\delta r = 0.5$, $A = 0.075$, $\omega = 1.025 \times 10^{-4}$, and $\alpha_m/\alpha_d = 15$. At this value of ω, the ordered system has no edge transport,

FIG. 13. x position vs ac cycle number n for a single skyrmion in a system with x direction driving, $n_{sk} = n_\phi = 0.4$, $\omega = 3.75 \times 10^{-5}$, $A = 0.075$, $\delta r = 0.5$, and $\alpha_m/\alpha_d = 10$. The disorder causes the skyrmion to become localized for extended periods of time.

the edge current drops to zero for a period of time before becoming finite again. In Fig. 13, we show an example of this behavior in a sample with $\omega = 3.75 \times 10^{-5}$, $A = 0.075$, $\delta r = 0.5$, and $\alpha_m/\alpha_d = 10$, which exhibits pronounced edge transport when $\delta r = 0.0$. The plot of the x position of a single skyrmion versus ac cycle number n shows that there are several time intervals during which the skyrmion becomes localized. The edge skyrmions trace the same path during each ac cycle in the localized interval, but this path is chaotic, allowing the skyrmions eventually to jump back into a translating orbit.

In Fig. 14(a), we plot $\langle d \rangle$ versus δr for the system in Fig. 12(a), where we find an increase in the edge current for intermediate values of δr. For larger disorder, however, the transport is reduced due to the pinning of the edge current by the disorder. In Fig. 14(b), we show $\langle d \rangle$ versus δr for the system in Fig. 13 where the addition of disorder decreases the edge transport. We find similar effects for driving in the y direction.
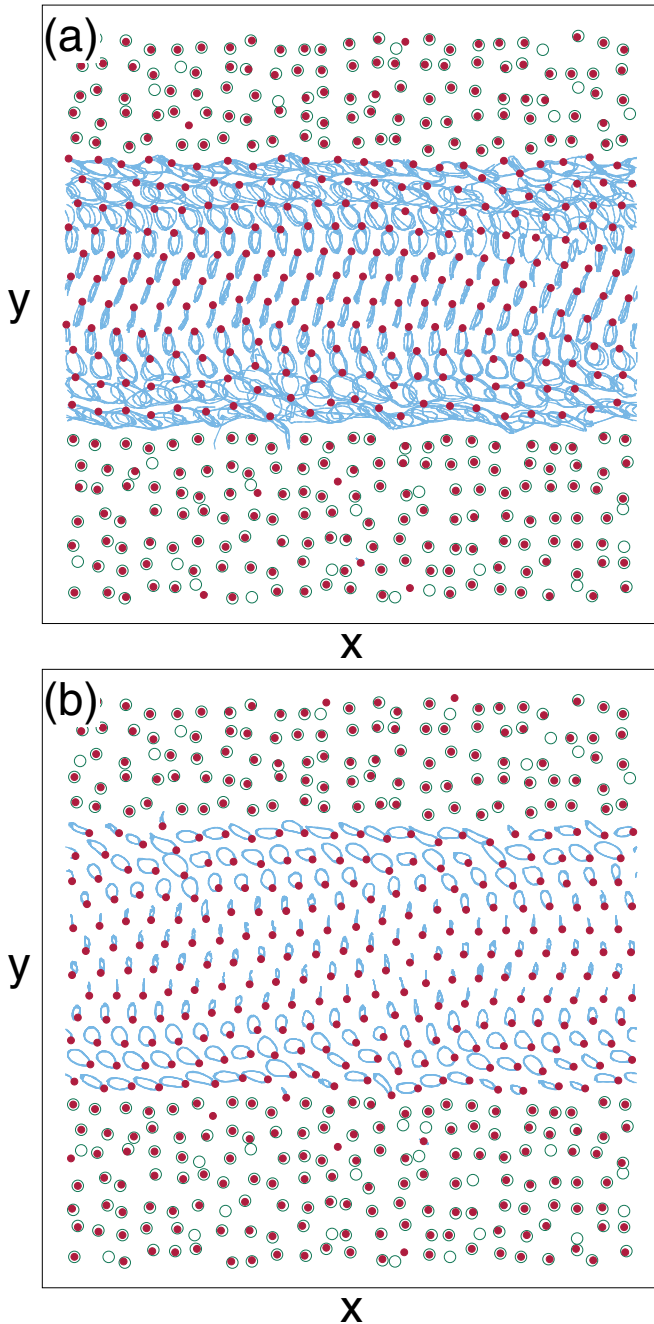
FIG. 12. Skyrmion positions (dots), trajectories (lines), and pinning site locations (open circles) for samples in which disorder has been added in the form of random offsets δr of the pinning site locations. Here, the driving is in the x direction and $n_{sk} = n_\phi = 0.4$. (a) Disorder-induced edge transport at $\omega = 1.025 \times 10^{-4}$, $A = 0.075$, $\alpha_m/\alpha_d = 15$, and $\delta r = 0.5$. (b) Localized lattice phase in the same system at $\omega = 1.5 \times 10^{-4}$, where there is no edge transport.

as shown in Fig. 5(b). In the presence of sufficiently large disorder, however, edge transport occurs in the two edgemost rows. Figure 12(b) shows the same sample at a higher ac drive frequency of $\omega = 1.5 \times 10^{-4}$, where the orbits are small enough that the edge currents are lost even in the presence of disorder.

In other cases, the addition of disorder reduces the edge currents and produces intermittent or chaotic motion in which
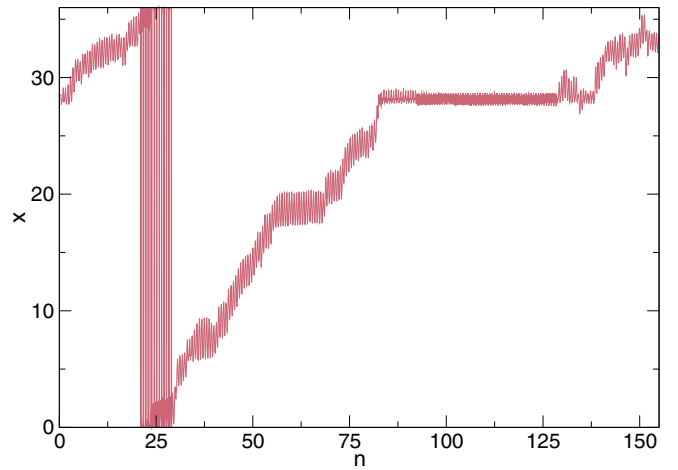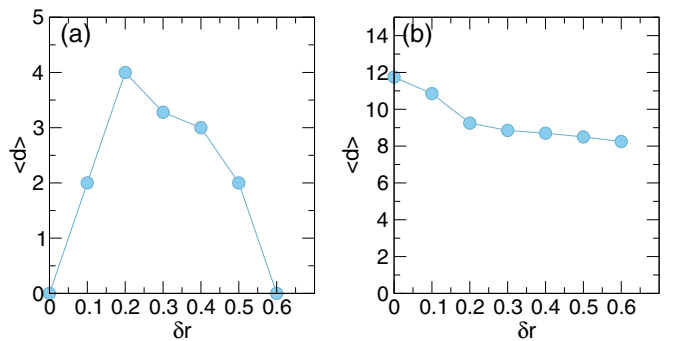

FIG. 14. $\langle d \rangle$ vs δr for the system in Fig. 12(a) with x direction driving showing that addition of disorder can induce an edge current. Here, $n_{sk} = n_\phi = 0.4$, $\omega = 1.025 \times 10^{-4}$, $A = 0.075$, and $\alpha_m/\alpha_d = 15$. (b) $\langle d \rangle$ vs δr for the system in Fig. 13 at $n_{sk} = n_\phi = 0.4$, $\omega = 3.75 \times 10^{-5}$, $A = 0.075$, and $\alpha_m/\alpha_d = 10$, where addition of disorder reduces the edge current.
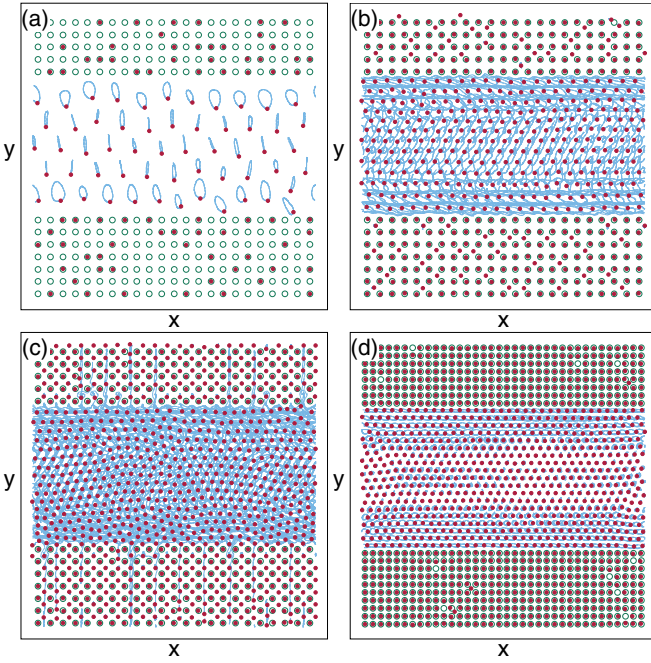
FIG. 15. Skyrmion positions (dots), trajectories (lines), and pinning site locations (open circles) for a system with x direction driving at $A = 0.075$, $\omega = 3.75 \times 10^{-5}$, and $\alpha_m/\alpha_d = 10$ for fixed matching density $n_\phi = 0.4$ and varied skyrmion density. (a) In the localized lattice phase at $n_{sk} = 0.1$, there is no edge current. (b) In the edge transport phase at $n_{sk} = 0.5$, there is strong edge transport. (c) In the edge transport phase at $n_{sk} = 1.0$, there is considerable disorder in the trajectories and the edge transport is reduced. (d) The edge transport phase in a system with a matching density of $n_\phi = 1.0$ and skyrmion density $n_{sk} = 1.0$ for $A = 0.25$, $\omega = 3.75 \times 10^{-5}$, and $\alpha_m/\alpha_d = 10$.

VI. DENSITY AND SKYRMION PUMPING EFFECTS

To determine the effects of changing the skyrmion density, we study both the case in which the pinning density is held fixed and the skyrmion density is varied, as well as the case in which the ratio of the number of pins to the number of skyrmions is held fixed at $N_p/N_{sk} = 1/2$ but the matching density n_ϕ of the system is changed. In Fig. 15(a), we plot the skyrmion trajectories at $\alpha_m/\alpha_d = 10$, $A = 0.075$, and $\omega = 3.75 \times 10^{-5}$ at a skyrmion density of $n_{sk} = 0.1$ and a fixed matching density of $n_\phi = 0.4$. The skyrmion density is low enough that no edge transport occurs. Figure 15(b) shows the same system at $n_{sk} = 0.5$ where there is strong edge transport, and Fig. 15(c) illustrates the trajectories at $n_{sk} = 1.0$, where the edge transport is reduced and there is an increase in the motion of interstitial skyrmions within the pinned region. In Fig. 15(d), the matching density is increased to $n_\phi = 1.0$ and the skyrmion density is $n_{sk} = 1.0$. Here, at $A = 0.025$ and $\omega = 3.75 \times 10^{-5}$, edge currents are present. In Fig. 16(a), we plot $\langle d \rangle$ versus n_{sk} for the system in Fig. 15 with a fixed matching density of $n_\phi = 0.4$. For $n_{sk} < 0.15$, there is no edge current, while for $0.4 < n_{sk} < 0.8$, pronounced edge transport appears which falls off when $n_{sk} > 0.8$. The decrease in the edge transport with increasing n_{sk} at higher densities occurs because the number of interstitial skyrmions in the pinned region is increasing, contributing a fluctuating
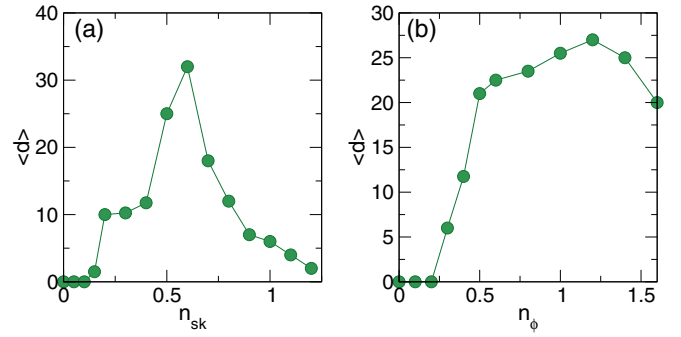

FIG. 16. (a) $\langle d \rangle$ vs n_{sk} for a system with a fixed matching density of $n_\phi = 0.4$ under x direction driving at $\omega = 3.75 \times 10^{-5}$, $A = 0.075$, and $\alpha_m/\alpha_d = 10$. The edge currents are lost at low skyrmion density and diminish with increasing n_{sk} at high skyrmion density. (b) $\langle d \rangle$ vs the matching density n_ϕ in samples with $n_{sk} = n_\phi$, $\omega = 3.75 \times 10^{-5}$, $A = 0.075$, and $\alpha_m/\alpha_d = 10$, showing that the edge transport is robust over a wide range of system densities.

component of increasing magnitude to the edge potential. In addition, at higher skyrmion densities, the skyrmion orbits become compressed due to the decrease in the skyrmion lattice constant. This effect is similar to what we find for reduced ac amplitude or higher ac drive frequencies, both of which suppress the edge transport. The peak value in $\langle d \rangle$ is produced by a resonance effect in which the width of the skyrmion orbits along the channel edge locks to the periodicity of the confining potential created by the pinned skyrmions.

In Fig. 17, we plot the x position of a single skyrmion on the lower edge of the pin-free region in the system from Figs. 15(a)–15(c) with $n_\phi = 0.4$ at three different skyrmion densities. At $n_{sk} = 0.1$, the skyrmion undergoes a brief transient motion before becoming localized. When $n_{sk} = 0.5$, the skyrmion translates rapidly, moving nearly one pinning lattice constant per ac cycle, giving a transport that is close to optimal. At $n_{sk} = 1.0$, the edge current is strongly reduced.
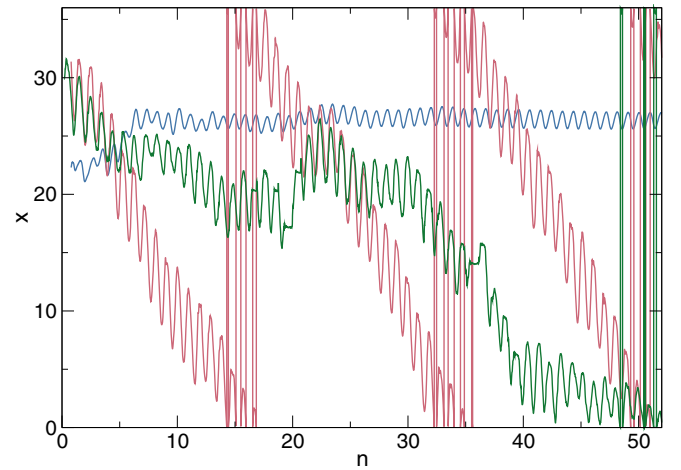
FIG. 17. x positions vs ac cycle number n for an individual skyrmion on the lower edge of the pin-free channel in the system from Figs. 15(a)–15(c) with x direction driving at $A = 0.075$, $\omega = 3.75 \times 10^{-5}$, $\alpha_m/\alpha_d = 10$, and $n_\phi = 0.4$. When $n_{sk} = 0.1$ (blue), the skyrmion is localized. For $n_{sk} = 0.5$ (red), there is strong edge transport, while at $n_{sk} = 1.0$ (green) the edge transport is reduced.
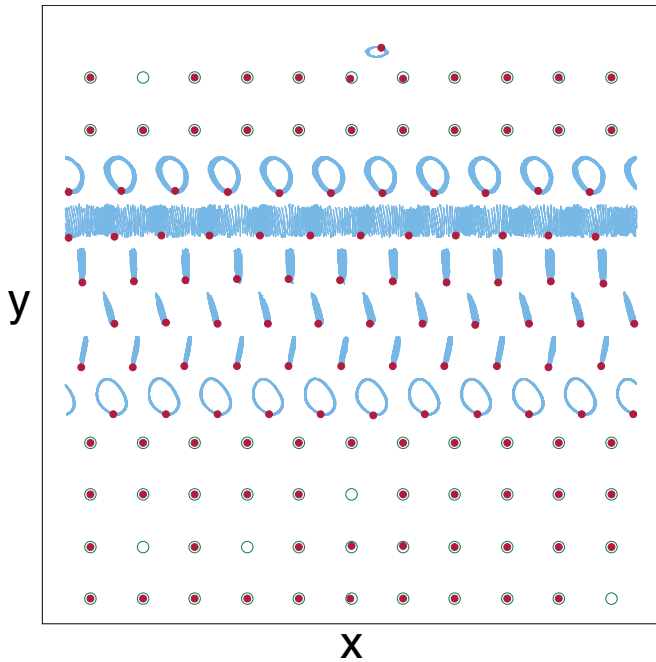
FIG. 18. Skyrmion positions (dots), trajectories (lines), and pinning site locations (open circles) for a system with x direction driving and a matching density of $n_\phi = 0.1$ at $n_{sk} = 0.1$, $A = 0.075$, $\omega = 3.75 \times 10^{-5}$, and $\alpha_m/\alpha_d = 10$. A different type of current, termed a skyrmion pump effect, occurs in the second row from the top of the pin-free channel. The skyrmion pump effect appears due to an incommensuration between this second row and the row at the upper edge of the pin-free channel. The skyrmions are propagating in the negative x-direction, opposite to the edge current motion that appears for higher n_ϕ.

In Fig. 16(b), we plot $\langle d \rangle$ versus the matching density n_ϕ in samples with $n_{sk} = n_\phi$ for the same parameters as in Fig. 16(a). Here, a finite edge current appears only when $n_\phi > 0.3$, and the edge transport remains robust as n_ϕ is further increased. This result indicates that edge currents should be a general effect which can be observed whenever collective interactions between the skyrmions are important.

Although we do not find any edge transport when $n_\phi < 0.3$, we observe a different type of translating orbit that we call a skyrmion pump effect. In Fig. 18, we illustrate the pump effect in a sample with $n_\phi = 0.1$, $n_{sk} = 0.1$, $A = 0.075$, $\omega = 3.75 \times 10^{-5}$, and $\alpha_m/\alpha_d = 10.0$. The skyrmion trajectories, obtained over a time period of $n = 250$ cycles, indicate that the skyrmions in the second row from the top of the pin-free channel are undergoing transport, while the top row remains localized. The pump effect flow is much slower than the edge transport motion found at higher n_ϕ and it is also oriented in the opposite direction, with skyrmions moving in the negative x direction instead of in the positive x direction. In Fig. 19, we plot the x position versus ac drive cycle number n for a skyrmion in the second row from the top of the pin-free channel in the system from Fig. 18. The skyrmion is moving in the negative x direction and exhibits x position oscillations which are much smaller than those found for edge transport. For comparison, we also plot the x position of a skyrmion in the top row of the pin-free channel, which becomes localized
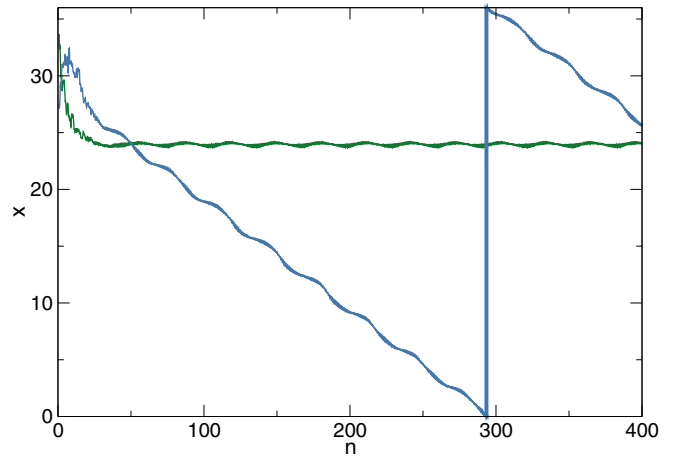

FIG. 19. x position vs ac cycle number n for a skyrmion in the second row from the top of the pin-free channel (blue) and a skyrmion in the top row (green) for the system in Fig. 18 with x direction driving at $n_{sk} = n_\phi = 0.1$, $A = 0.075$, $\omega = 3.75 \times 10^{-5}$, and $\alpha_m/\alpha_d = 10$. The pumped skyrmion is moving in the $-x$ direction, which is opposite to the direction of motion found for edge transport of the top row at higher n_ϕ.

after an initial transient motion. The skyrmion pump effect arises when the number of skyrmions in the top row of the pin-free channel is incommensurate with the number of skyrmions in the adjacent row. Here, the top row contains 11 skyrmions while the second row from the top contains 12 skyrmions. In contrast, both of the bottom two rows in the pin-free channel contain 11 skyrmions. The incommensuration causes the skyrmions in the top row to act as an effective gear that gradually translates the skyrmions in the second row from the top. If the number of skyrmions in the adjacent row is smaller rather than larger than the number of skyrmions in the top row (10 skyrmions instead of 12), the pump flow direction is reversed. We observe the pump effect when $0.05 < n_\phi < 0.2$ in samples with $n_{sk} = n_\phi$, and it is always associated with an incommensuration between the edge row and an adjacent row. For small densities $n_\phi \leqslant 0.05$, the skyrmions are so far apart that their interactions become unimportant and the pump effect disappears. We note that a similar pump effect could also occur at higher densities $n_\phi \geqslant 0.2$ where edge transport appears; however, since the pump effect is very weak, it is difficult to detect in the presence of the much stronger edge transport.

VII. DISCUSSION

Edge states have previously been proposed to occur in skyrmion systems, such as for frustrated magnets [73] where a dc current can induce motion on the edges of the sample; however, this effect is very different from the edge transport we propose here and it occurs due to a different mechanism. Chiral magnonic edge states for antiferromagnetic skyrmion crystals have also been proposed [74], but these differ from the edge current and skyrmion transport that we consider here. We note that our results do show similarities with recent studies of edge transport in chiral active matter or active spinning systems, where directed transport can occur near the edge of the sample or between regions of spinners of opposite chirality

[7]. There are still several differences in that the chiral active spinning particles always undergo circular motion, whereas in the absence of confinement, skyrmions subjected to an ac drive move along 1D paths, with circular orbits appearing only due to the presence of a confining potential or similar quenched disorder. The pinning potential we consider is produced by pinned skyrmions; however, it is possible to create other types of confining potentials, such as by using nanoscale pinning sites that repel skyrmions, by modifying the materials properties along the edges or in stripe patterns [75,76], or by using nanowires with rough edges [77].

Beyond nanostructured geometries, our work suggests that skyrmion edge transport could also be observed at the interface between lattices of two different skyrmion species, between skyrmions with different chiralities [78], or along grain boundaries or regions of coexisting skyrmion and helical states [79–82]. In Fig. 20(a), we illustrate an example of an edge state that appears in a pin-free system at the interface between different skyrmion species. We consider a system with $\alpha_m/\alpha_d = 10$, $\omega = 1.25 \times 10^{-4}$, $A = 0.075$, and $n_{sk} = 0.2$ where half of the skyrmions have a Magnus term that is opposite in sign to the other half of the skyrmions. The skyrmions of opposite sign are placed in a band aligned with the x direction. Under an ac drive applied in the x direction, elliptical orbits appear along the domain boundaries separating the two species, while in the bulk of each domain, the skyrmions follow 1D trajectories. In Fig. 20(b), we show the same system at $n_{sk} = 0.4$, where clear edge currents emerge at the boundaries between the species.

Other methods of introducing confining boundaries in the sample include using inhomogeneous pinning strength so that skyrmions in one region of the sample are more strongly (or less strongly) pinned than skyrmions in adjacent regions. It would be interesting to examine the effects of confinement on different types of skyrmions, such as antiferromagnetic skyrmions [83–85]. If the Magnus force is absent, the skyrmion dynamics would be consistent with what is found in an overdamped system and the edge transport would be absent. There are also other possible systems that could exhibit edge currents, such as the trochoidal motion of skyrmions in certain bilayer systems [60] as well as the dynamics of antiskyrmion lattices [85], meron lattices [86], or polar skyrmions [87].

In this work, we considered only a single ac drive applied either parallel or perpendicular to the pin-free channel. It is possible, however, to apply more complex ac drives such as $\mathbf{F}^{ac} = A\sin(\omega t)\hat{\mathbf{x}} + A\cos(\omega t)\hat{\mathbf{y}}$. A circular ac drive of this type applied to an underdamped system can create commensurate-incommensurate transitions and localized or delocalized states in the presence of periodic or random disorder [69,88]. Addition of an asymmetry in either the substrate or the circular orbit itself can produce directed motion in the overdamped system [67,89–91], so a rich array of phenomena is expected to appear for skyrmions under multiple ac drives. For example, ratcheting skyrmion motion was observed in work on biharmonic drives [57]. In Fig. 21(a), we show the trajectories for a skyrmion system with $n_\phi = 0.1$, $n_{sk} = n_\phi$, $\alpha_m/\alpha_d = 10$, $A = 0.075$, and $\omega = 3.75 \times 10^{-5}$ under a circular ac drive. In this case, there is no edge current; however, the skyrmions in the bulk of the pin-free channel
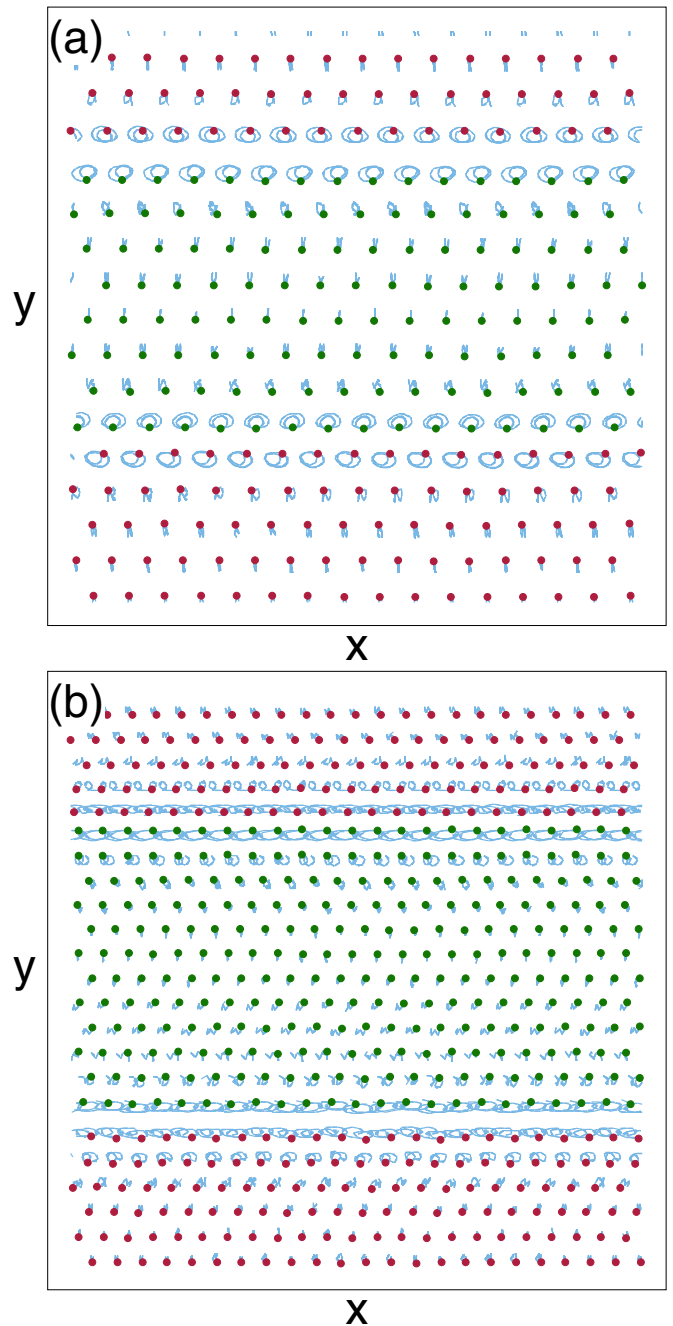

FIG. 20. Skyrmion positions (dots) and trajectories (lines) in a system with x direction driving and no pinning containing two different skyrmion species (red and green) that have Magnus terms of the opposite sign. (a) At $n_{sk} = 0.2$, $\alpha_m/\alpha_d = 10$, $A = 0.075$, and $\omega = 1.25 \times 10^{-4}$, the largest circular orbits appear along the boundary between the two species. (b) For the same parameters but at $n_{sk} = 0.4$, edge currents are flowing along the domain walls separating the two species.

follow orbits that are much more circular than the orbits of the skyrmions at the edges of the channel, in contrast to what we find for a linear ac drive. In Fig. 21(b), the same system at a matching density of $n = 0.2$ exhibits edge currents, with particularly rapid transport occurring along the lower edge of the pin-free channel.
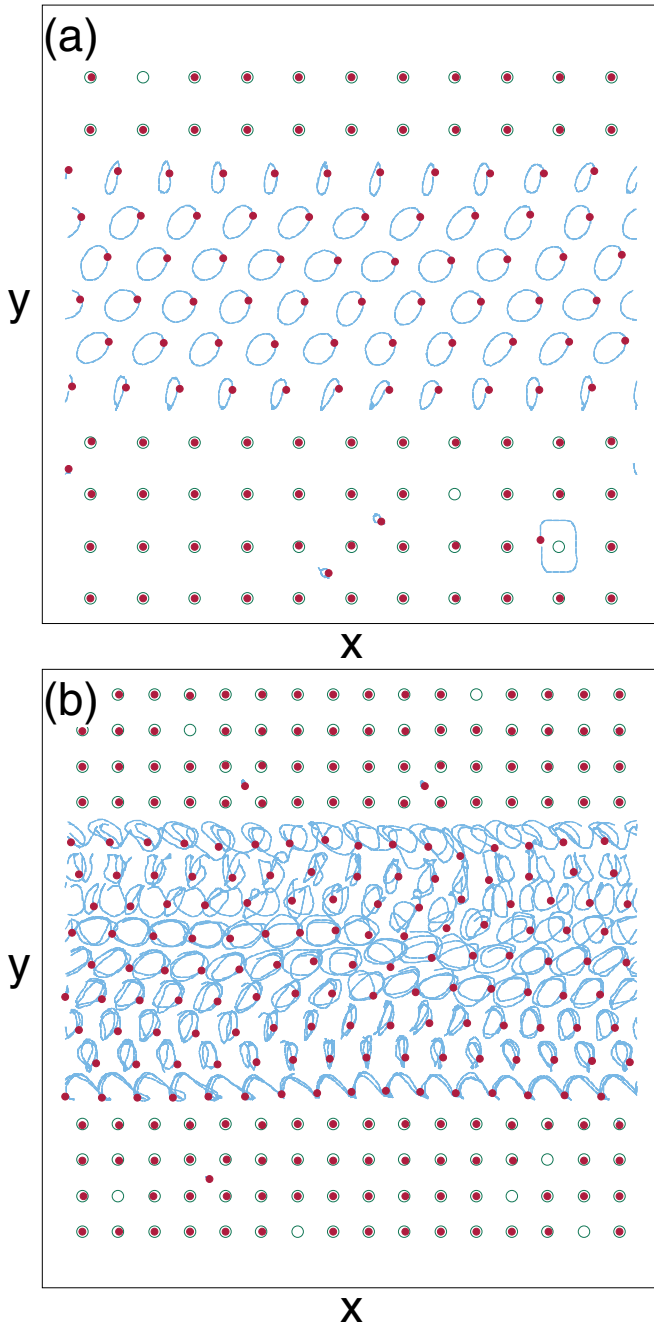
FIG. 21. Skyrmion positions (dots), trajectories (lines), and pinning site locations (open circles) for a system with a circular ac drive applied along the x direction. (a) At $\alpha_m/\alpha_d = 10$, $A = 0.075$, $\omega = 3.75 \times 10^{-5}$, $n_\phi = 0.1$, and $n_{sk} = n_\phi$, the orbits are localized. (b) In the same system at $n_\phi = 0.2$ and $n_{sk} = n_\phi$, edge currents are present.

Studies of gyroscopic metamaterials [11,13,14] showed that perturbations migrate to the edge of the sample and propagate around the edge in one direction. In our system, for very weak damping or small α_m, it would be possible to perturb skyrmions in the bulk of the pin-free channel and obtain motion that is localized on the edges of the channel, producing a transient current which eventually damps away. Since the skyrmion lattice has many similarities to gyroscopic metama-

terials, other effects observed in the latter system could be relevant for skyrmions in confinement, such as the odd viscosity and odd elasticity found in driven chiral matter [92–94].

It would also be possible to use an edge current to create a device. For example, in a race track geometry filled with a skyrmion lattice, an ac drive could cause a signal to propagate along the edge of the race track. One advantage of this mode of operation is that the propagating skyrmions will exhibit a skyrmion Hall angle equal to zero, eliminating the problem of having skyrmions escape from the edges of the track as they move. Our results suggest that the propagation speed of the signal will not monotonically increase with increasing ac frequency, but will instead drop to zero at high frequencies. In our work, we have considered only rigid skyrmions, but in continuum systems, additional edge modes could arise such as the prorogation of breathing modes or perturbations of the internal modes of the skyrmions.

VIII. SUMMARY

In summary, we have shown that for a skyrmion lattice in a confining pinned geometry, application of an ac drive combined with the intrinsic Magnus force produces circular orbits of skyrmions near the edge of the pin-free channel. This can generate an edge current of skyrmions in which the direction of transport is controlled by the sign of the Magnus force and the orientation of the edge. Simultaneously, skyrmions in the bulk of the pin-free channel are localized and follow closed periodic orbits. The magnitude of the edge current depends on the ratio of the Magnus force to the damping term as well as on the amplitude and frequency of the ac drive. We identify three dynamic phases: A localized state in which no edge transport occurs, a lattice state with edge transport, and a disordered fluctuating state that appears for high ac drive amplitude. In regimes where the edge transport is strong, the transport can extend beyond the edges and can involve one or two additional rows of skyrmions adjacent to the edgemost row. In the overdamped limit, the skyrmion orbits become one-dimensional and the edge transport is lost. The edge currents are the most pronounced when the ac drive is parallel to the pin-free channel since the Magnus force induces motion perpendicular to the driving direction. A parallel drive pushes the skyrmions against the edges of the confining potential and induces the circular orbits that are necessary to generate the edge transport. In contrast, when the ac drive is applied perpendicular to the pin-free channel, the motion of the skyrmions is more one dimensional, the coupling to the confining potential is reduced, and the edge transport is diminished. We show that these results are robust against disorder and that in some cases the addition of disorder can induce edge transport. For lower skyrmion densities, we observe a skyrmion pump effect produced by an incommensuration between the number of skyrmions in the row at the edge of the pin-free channel and the number of skyrmions in the adjacent pin-free row. The emergence of edge currents should be a generic feature of driven or excited skyrmion lattices that are subjected to confinement or that contain an interface, and as an example we demonstrate that an ac drive can induce edge transport along the domain boundary separating two different species of skyrmions.

[1] E. Teller, Diamagnetism of free electrons, Z. Phys. **67**, 311 (1931).

[2] B. I. Halperin, Quantized Hall conductance, current-carrying edge states, and the existence of extended states in a two-dimensional disordered potential, Phys. Rev. B **25**, 2185 (1982).

[3] C. W. J. Beenakker, H. van Houten, and B. J. van Wees, Skipping orbits, traversing trajectories, and quantum ballistic transport in microstructures, Superlattices Microstruct. **5**, 127 (1989).

[4] J. E. Müller, Effect of a Nonuniform Magnetic Field on a Two-Dimensional Electron Gas in the Ballistic Regime, Phys. Rev. Lett. **68**, 385 (1992).

[5] J. Reijniers, A. Matulis, K. Chang, F. M. Peeters, and P. Vasilopoulos, Confined magnetic guiding orbit states, Europhys. Lett. **59**, 749 (2002).

[6] B. K. Stuhl, H. I. Lu, L. M. Aycock, D. Genkina, and I. B. Spielman, Visualizing edge states with an atomic Bose gas in the quantum Hall regime, Science **349**, 1514 (2015).

[7] B. C. van Zuiden, J. Paulose, W. T. M. Irvine, D. Bartolo, and V. Vitelli, Spatiotemporal order and emergent edge currents in active spinner materials, Proc. Natl. Acad. Sci. USA **113**, 12919 (2016).

[8] M. Han, J. Yan, S. Granick, and E. Luijten, Effective temperature concept evaluated in an active colloid mixture, Proc. Natl. Acad. Sci. USA **114**, 7513 (2017).

[9] K. Dasbiswas, K. K. Mandadapu, and S. Vaikuntanathan, Topological localization in out-of-equilibrium dissipative systems, Proc. Natl. Acad. Sci. USA **115**, E9031 (2018).

[10] C. Reichhardt and C. J. O. Reichhardt, Reversibility, pattern formation, and edge transport in active chiral and passive disk mixtures, J. Chem. Phys. **150**, 064905 (2019).

[11] L. M. Nash, D. Kleckner, A. Read, V. Vitelli, A. M. Turner, and W. T. M. Irvine, Topological mechanics of gyroscopic metamaterials, Proc. Natl. Acad. Sci. USA **112**, 14495 (2015).

[12] R. Süsstrunk and S. D. Huber, Observation of phononic helical edge states in a mechanical topological insulator, Science **349**, 47 (2015).

[13] N. P. Mitchell, L. M. Nash, D. Hexner, A. M. Turner, and W. T. M. Irvine, Amorphous topological insulators constructed from random point sets, Nat. Phys. **14**, 380 (2018).

[14] N. P. Mitchell, L. M. Nash, and W. T. M. Irvine, Realization of a topological phase transition in a gyroscopic lattice, Phys. Rev. B **97**, 100302(R) (2018).

[15] J. Loehr, M. Loenne, A. Ernst, D. de las Heras, and T. M. Fischer, Topological protection of multiparticle dissipative transport, Nat. Commun. **7**, 11745 (2016).

[16] J. Loehr, D. de las Heras, A. Jarosz, M. Urbaniak, F. Stobiecki, A. Tomita, R. Huhnstock, I. Koch, A. Ehresmann, D. Holzinger, and T. M. Fischer, Colloidal topological insulators, Commun. Phys. **1**, 4 (2018).

[17] M. Z. Hasan and C. L. Kane, Colloquium: Topological insulators, Rev. Mod. Phys. **82**, 3045 (2010).

[18] N. Nagaosa and Y. Tokura, Topological properties and dynamics of magnetic skyrmions, Nat. Nanotechnol. **8**, 899 (2013).

[19] K. Everschor-Sitte, J. Masell, R. M. Reeve, and M. Kläui, Perspective: Magnetic skyrmions-overview of recent progress in an active research field, J. Appl. Phys. **124**, 240901 (2018).

[20] A. N. Bogdanov and D. A. Yablonskii, Thermodynamically stable 'vortices' in magnetically ordered crystals. The mixed state of magnets, Sov. Phys. JETP **68**, 101 (1989).

[21] S. Mühlbauer, B. Binz, F. Jonietz, C. Pfleiderer, A. Rosch, A. Neubauer, R. Georgii, and P. Böni, Skyrmion lattice in a chiral magnet, Science **323**, 915 (2009).

[22] X. Z. Yu, Y. Onose, N. Kanazawa, J. H. Park, J. H. Han, Y. Matsui, N. Nagaosa, and Y. Tokura, Real-space observation of a two-dimensional skyrmion crystal, Nature (London) **465**, 901 (2010).

[23] W. Jiang, P. Upadhyaya, W. Zhang, G. Yu, M. B. Jungfleisch, F. Y. Fradin, J. E. Pearson, Y. Tserkovnyak, K. L. Wang, O. Heinonen, S. G. E. te Velthuis, and A. Hoffmann, Blowing magnetic skyrmion bubbles, Science **349**, 283 (2015).

[24] Y. Tokunaga, X. Z. Yu, J. S. White, H. M. Rønnow, D. Morikawa, Y. Taguchi, and Y. Tokura, A new class of chiral materials hosting magnetic skyrmions beyond room temperature, Nat. Commun. **6**, 7638 (2015).

[25] S. Woo, K. Litzius, B. Krüger, M.-Y. Im, L. Caretta, K. Richter, M. Mann, A. Krone, R. M. Reeve, M. Weigand, P. Agrawal, I. Lemesh, M.-A. Mawass, P. Fischer, M. Kläui, and G. S. D. Beach, Observation of room-temperature magnetic skyrmions and their current-driven dynamics in ultrathin metallic ferromagnets, Nat. Mater. **15**, 501+ (2016).

[26] A. Soumyanarayanan, M. Raju, A. L. Gonzalez Oyarce, Anthony K. C. Tan, M.-Y. Im, A. P. Petrovic, P. Ho, K. H. Khoo, M. Tran, C. K. Gan, F. Ernult, and C. Panagopoulos, Tunable room-temperature magnetic skyrmions in Ir/Fe/Co/Pt multilayers, Nat. Mater. **16**, 898 (2017).

[27] W. Jiang, G. Chen, K. Liu, J. Zang, S. G. E. te Velthuis, and A. Hoffmann, Skyrmions in magnetic multilayers, Phys. Rep. **704**, 1 (2017).

[28] T. Schulz, R. Ritz, A. Bauer, M. Halder, M. Wagner, C. Franz, C. Pfleiderer, K. Everschor, M. Garst, and A. Rosch, Emergent electrodynamics of skyrmions in a chiral magnet, Nat. Phys. **8**, 301 (2012).

[29] X. Z. Yu, N. Kanazawa, W. Z. Zhang, T. Nagai, T. Hara, K. Kimoto, Y. Matsui, Y. Onose, and Y. Tokura, Skyrmion flow near room temperature in an ultralow current density, Nat. Commun. **3**, 988 (2012).

[30] J. Iwasaki, M. Mochizuki, and N. Nagaosa, Universal current-velocity relation of skyrmion motion in chiral magnets, Nat. Commun. **4**, 1463 (2013).

[31] S.-Z. Lin, C. Reichhardt, C. D. Batista, and A. Saxena, Driven Skyrmions and Dynamical Transitions in Chiral Magnets, Phys. Rev. Lett. **110**, 207202 (2013).

[32] D. Liang, J. P. DeGrave, M. J. Stolt, Y. Tokura, and S. Jin, Current-driven dynamics of skyrmions stabilized in MnSi nanowires revealed by topological Hall effect, Nat. Commun. **6**, 8217 (2015).

[33] W. Legrand, D. Maccariello, N. Reyren, K. Garcia, C. Moutafis, C. Moreau-Luchaire, S. Coffin, K. Bouzehouane, V. Cros, and A. Fert, Room-temperature current-induced generation and motion of sub-100 nm skyrmions, Nano Lett. **17**, 2703 (2017).

[34] R. Tolley, S. A. Montoya, and E. E. Fullerton, Room-temperature observation and current control of skyrmions in Pt/Co/Os/Pt thin films, Phys. Rev. Mater. **2**, 044404 (2018).

[35] C. Reichhardt and C. J. Olson Reichhardt, Depinning and nonequilibrium dynamic phases of particle assemblies driven over random and ordered substrates: A review, Rep. Prog. Phys. **80**, 026501 (2017).

[36] A. Fert, V. Cros, and J. Sampaio, Skyrmions on the track, Nat. Nanotechnol. **8**, 152 (2013).

[37] R. Tomasello, E. Martinez, R. Zivieri, L. Torres, M. Carpentieri, and G. Finocchio, A strategy for the design of skyrmion racetrack memories, Sci. Rep. **4**, 6784 (2014).

[38] A. Fert, N. Reyren, and V. Cros, Magnetic skyrmions: Advances in physics and potential applications, Nat. Rev. Mater. **2**, 17031 (2017).

[39] J. Zázvorka, F. Jakobs, D. Heinze, N. Keil, S. Kromin, S. Jaiswal, K. Litzius, G. Jakob, P. Virnau, D. Pinna, K. Everschor-Sitte, L. Rózsa, A. Donges, U. Nowak, and M. Kläui, Thermal skyrmion diffusion used in a reshuffler device, Nat. Nanotechnol. **14**, 658 (2019).

[40] S.-Z. Lin, C. Reichhardt, C. D. Batista, and A. Saxena, Particle model for skyrmions in metallic chiral magnets: Dynamics, pinning, and creep, Phys. Rev. B **87**, 214419 (2013).

[41] C. Reichhardt, D. Ray, and C. J. Olson Reichhardt, Collective Transport Properties of Driven Skyrmions with Random Disorder, Phys. Rev. Lett. **114**, 217202 (2015).

[42] C. Reichhardt and C. J. Olson Reichhardt, Noise fluctuations and drive dependence of the skyrmion Hall effect in disordered systems, New J. Phys. **18**, 095005 (2016).

[43] J.-V. Kim and M.-W. Yoo, Current-driven skyrmion dynamics in disordered films, Appl. Phys. Lett. **110**, 132404 (2017).

[44] W. Jiang, X. Zhang, G. Yu, W. Zhang, X. Wang, M. B. Jungfleisch, J. E. Pearson, X. Cheng, O. Heinonen, K. L. Wang, Y. Zhou, A. Hoffmann, and S. G. E. te Velthuis, Direct observation of the skyrmion Hall effect, Nat. Phys. **13**, 162 (2017).

[45] K. Litzius, I. Lemesh, B. Krüger, P. Bassirian, L. Caretta, K. Richter, F. Büttner, K. Sato, O. A. Tretiakov, J. Förster, R. M. Reeve, M. Weigand, L. Bykova, H. Stoll, G. Schütz, G. S. D. Beach, and M. Kläui, Skyrmion Hall effect revealed by direct time-resolved X-ray microscopy, Nat. Phys. **13**, 170 (2017).

[46] S. Woo, K. M. Song, X. C. Zhang, Y. Zhou, M. Ezawa, X. X. Liu, S. Finizio, J. Raabe, N. J. Lee, S.-I. Kim, S.-Y. Park, Y. Kim, J.-Y. Kim, D. Lee, O. Lee, J. W. Choi, B.-C. Min, H. C. Koo, and J. Chang, Current-driven dynamics and inhibition of the skyrmion Hall effect of ferrimagnetic skyrmions in GdFeCo films, Nat. Commun. **9**, 959 (2018).

[47] R. Juge, S.-G. Je, D. de Souza Chaves, L. D. Buda-Prejbeanu, J. Peña-Garcia, J. Nath, I. M. Miron, K. G. Rana, L. Aballe, M. Foerster, F. Genuzio, T. O. Mentes, A. Locatelli, F. Maccherozzi, S. S. Dhesi, M. Belmeguenai, Y. Roussigné, S. Auffret, S. Pizzini, G. Gaudin *et al.*, Current-driven dynamics

of magnetic skyrmions in an ultrathin film: Experiments and modelling, Phys. Rev. Appl. **12**, 044007 (2019).

[48] K. Zeissler, S. Finizio, C. Barton, A. Huxtable, J. Massey, J. Raabe, A. V. Sadovnikov, S. A. Nikitov, R. Brearton, T. Hesjedal, G. van der Laan, M. C. Rosamond, E. H. Linfield, G. Burnell, and C. H. Marrows, Diameter-independent skyrmion Hall angle in the plastic flow regime observed in chiral magnetic multilayers, arXiv:1908.04239.

[49] Y.-H. Liu and Y.-Q. Li, A mechanism to pin skyrmions in chiral magnets, J. Phys.: Condens. Matter **25**, 076005 (2013).

[50] S.-Z. Lin, C. Reichhardt, and A. Saxena, Manipulation of skyrmions in nanodisks with a current pulse and skyrmion rectifier, Appl. Phys. Lett. **102**, 222405 (2013).

[51] J. Müller and A. Rosch, Capturing of a magnetic skyrmion with a hole, Phys. Rev. B **91**, 054410 (2015).

[52] F. Büttner, C. Moutafis, M. Schneider, B. Krüger, C. M. Günther, J. Geilhufe, C. von Kor Schmising, J. Mohanty, B. Pfau, S. Schaffert, A. Bisig, M. Foerster, T. Schulz, C. A. F. Vaz, J. H. Franken, H. J. M. Swagten, M. Kläui, and S. Eisebitt, Dynamics and inertia of skyrmionic spin structures, Nat. Phys. **11**, 225 (2015).

[53] C. Navau, N. Del-Valle, and A. Sanchez, Analytical trajectories of skyrmions in confined geometries: Skyrmionic racetracks and nano-oscillators, Phys. Rev. B **94**, 184104 (2016).

[54] L. González-Gómez, J. Castell-Queralt, N. Del-Valle, A. Sanchez, and C. Navau, Analytical modeling of the interaction between skyrmions and extended defects, Phys. Rev. B **100**, 054440 (2019).

[55] Y. Liu, N. Lei, C. Wang, X. Zhang, W. Kang, D. Zhu, Y. Zhou, X. Liu, Y. Zhang, and W. Zhao, Voltage-driven high-speed skyrmion motion in a skyrmion-shift device, Phys. Rev. Appl. **11**, 014004 (2019).

[56] R. M. Menezes, J. F. S. Neto, Clécio C. de Souza Silva, and M. V. Milošević, Manipulation of magnetic skyrmions by superconducting vortices in ferromagnet-superconductor heterostructures, Phys. Rev. B **100**, 014431 (2019).

[57] W. Chen, L. Liu, Y. Ji, and Y. Zheng, Skyrmion ratchet effect driven by a biharmonic force, Phys. Rev. B **99**, 064431 (2019).

[58] K.-W. Moon, D.-H. Kim, S.-G. Je, B. S. Chun, W. Kim, Z. Q. Qiu, S.-B. Choe, and C. Hwang, Skyrmion motion driven by oscillating magnetic field, Sci. Rep. **6**, 20360 (2016).

[59] H. Y. Yuan, X. S. Wang, M.-H. Yung, and X. R. Wang, Wiggling skyrmion propagation under parametric pumping, Phys. Rev. B **99**, 014428 (2019).

[60] U. Ritzmann, S. von Malottki, J.-V. Kim, S. Heinze, J. Sinova, and B. Dupe, Trochoidal motion and pair generation in skyrmion and antiskyrmion dynamics under spin-orbit torques, Nat. Electron. **1**, 451 (2018).

[61] C. Reichhardt and C. J. Olson Reichhardt, Shapiro steps for skyrmion motion on a washboard potential with longitudinal and transverse ac drives, Phys. Rev. B **92**, 224432 (2015).

[62] C. Reichhardt and C. J. Olson Reichhardt, Magnus-induced dynamics of driven skyrmions on a quasi-one-dimensional periodic substrate, Phys. Rev. B **94**, 094413 (2016).

[63] C. Reichhardt and C. J. Olson Reichhardt, Shapiro spikes and negative mobility for skyrmion motion on quasi-one-dimensional periodic substrates, Phys. Rev. B **95**, 014412 (2017).

[64] B. L. Brown, U. C. Täuber, and M. Pleimling, Skyrmion relaxation dynamics in the presence of quenched disorder, Phys. Rev. B **100**, 024410 (2019).

[65] P. Reimann, Brownian motors: Noisy transport far from equilibrium, Phys. Rep. **361**, 57 (2002).

[66] C. Reichhardt, C. J. Olson, and M. B. Hastings, Rectification and Phase Locking for Particles on Symmetric two-dimensional periodic substrates, Phys. Rev. Lett. **89**, 024101 (2002).

[67] C. Reichhardt and C. J. Olson Reichhardt, Absolute transverse mobility and ratchet effect on periodic two-dimensional symmetric substrates, Phys. Rev. E **68**, 046102 (2003).

[68] C. Reichhardt, C. J. Olson Reichhardt, and M. B. Hastings, Nonlinear dynamics, rectification, and phase locking for particles on symmetrical two-dimensional periodic substrates with dc and circular ac drives, Phys. Rev. E **69**, 056115 (2004).

[69] C. Reichhardt and C. J. Olson Reichhardt, Ratchet effect and nonlinear transport for particles on random substrates with crossed ac drives, Phys. Rev. E **73**, 011102 (2006).

[70] C. Reichhardt and C. J. Olson Reichhardt, Dynamics and separation of circularly moving particles in asymmetrically patterned arrays, Phys. Rev. E **88**, 042306 (2013).

[71] C. Reichhardt, D. Ray, and C. J. Olson Reichhardt, Reversible ratchet effects for vortices in conformal pinning arrays, Phys. Rev. B **91**, 184502 (2015).

[72] C. Reichhardt, D. Ray, and C. J. Olson Reichhardt, Magnus-induced ratchet effects for skyrmions interacting with asymmetric substrates, New J. Phys. **17**, 073034 (2015).

[73] A. O. Leonov and M. Mostovoy, Edge states and skyrmion dynamics in nanostripes of frustrated magnets, Nat. Commun. **8**, 14394 (2017).

[74] S. A. Díaz, J. Klinovaja, and D. Loss, Topological Magnons and Edge States in Antiferromagnetic Skyrmion Crystals, Phys. Rev. Lett. **122**, 187203 (2019).

[75] D. Stosic, T. B. Ludermir, and M. V. Milošević, Pinning of magnetic skyrmions in a monolayer Co film on Pt(111): Theoretical characterization and exemplified utilization, Phys. Rev. B **96**, 214403 (2017).

[76] I. L. Fernandes, J. Bouaziz, S. Blügel, and S. Lounis, Universality of defect-skyrmion interaction profiles, Nat. Commun. **9**, 4395 (2018).

[77] H. Du, R. Che, L. Kong, X. Zhao, C. Jin, C. Wang, J. Yang, W. Ning, R. Li, C. Jin, X. Chen, J. Zang, Y. Zhang, and M. Tian, Edge-mediated skyrmion chain and its collective dynamics in a confined geometry, Nat. Commun. **6**, 8504 (2015).

[78] K. Shibata, X. Z. Yu, T. Hara, D. Morikawa, N. Kanazawa, K. Kimoto, S. Ishiwata, Y. Matsui, and Y. Tokura, Towards control of the size and helicity of skyrmions in helimagnetic alloys by spin-orbit coupling, Nat. Nanotechnol. **8**, 723 (2013).

[79] T. Matsumoto, Y.-G. So, Y. Kohno, H. Sawada, R. Ishikawa, Y. Ikuhara, and N. Shibata, Jointed magnetic skyrmion lattices at a small-angle grain boundary directly visualized by advanced electron microscopy, Sci. Rep. **6**, 35880 (2016).

[80] Z.-A. Li, F. Zheng, A. H. Tavabi, J. Caron, C. Jin, H. Du, A. Kovacs, M. Tian, M. Farle, and R. E. Dunin-Borkowski, Magnetic skyrmion formation at lattice defects and grain boundaries studied by quantitative off-axis electron holography, Nano Lett. **17**, 1395 (2017).

[81] S. Pöllath, J. Wild, L. Heinen, T. N. G. Meier, M. Kronseder, L. Tutsch, A. Bauer, H. Berger, C. Pfleiderer, J. Zweck, A. Rosch, and C. H. Back, Dynamical Defects in Rotating Magnetic Skyrmion Lattices, Phys. Rev. Lett. **118**, 207205 (2017).

[82] S. L. Zhang, W. W. Wang, D. M. Burn, H. Peng, H. Berger, A. Bauer, C. Pfleiderer, G. van der Laan, and T. Hesjedal, Manipulation of skyrmion motion by magnetic field gradients, Nat. Commun. **9**, 2115 (2018).

[83] J. Barker and O. A. Tretiakov, Static and Dynamical Properties of Antiferromagnetic Skyrmions in the Presence of Applied Current and Temperature, Phys. Rev. Lett. **116**, 147203 (2016).

[84] W. Legrand, D. Maccariello, F. Ajejas, S. Collin, A. Vecchiola, K. Bouzehouane, N. Reyren, V. Cross, and A. Fert, Room-temperature stabilization of antiferromagnetic skyrmions in synthetic antiferromagnets, Nat. Mater. (2019), doi:10.1038/s41563-019-0468-3.

[85] A. K. Nayak, V. Kumar, T. Ma, P. Werner, E. Pippel, R. Sahoo, F. Damay, U. K. Rößler, C. Felser, and S. S. P. Parkin, Magnetic antiskyrmions above room temperature in tetragonal Heusler materials, Nature (London) **548**, 561 (2017).

[86] X. Z. Yu, W. Koshibae, Y. Tokunaga, K. Shibata, Y. Taguchi, N. Nagaosa, and Y. Tokura, Transformation between meron and skyrmion topological spin textures in a chiral magnet, Nature (London) **564**, 95 (2018).

[87] S. Das, Y. L. Tang, Z. Hong, M. A. P. Goncalves, M. R. McCarter, C. Klewe, K. X. Nguyen, F. Gomez-Ortiz, P. Shafer, E. Arenholz, V. A. Stoica, S. L. Hsu, B. Wang, C. Ophus, J. F. Liu, C. T. Nelson, S. Saremi, B. Prasad, A. B. Mei, D. G. Schlom *et al.*, Observation of room-temperature polar skyrmions, Nature (London) **568**, 368 (2019).

[88] C. Reichhardt and C. J. Olson, Vortex pinball under crossed ac drives in superconductors with periodic pinning arrays, Phys. Rev. B **65**, 100501(R) (2002).

[89] A. Soba, P. Tierno, T. M. Fischer, and F. Saguès, Dynamics of a paramagnetic colloidal particle driven on a magnetic-bubble lattice, Phys. Rev. E **77**, 060401(R) (2008).

[90] D. Speer, R. Eichhorn, and P. Reimann, Directing Brownian Motion on a Periodic Surface, Phys. Rev. Lett. **102**, 124101 (2009).

[91] R. Chacón and A. M. Lacasta, Controlling chaotic transport in two-dimensional periodic potentials, Phys. Rev. E **82**, 046207 (2010).

[92] D. Banerjee, A. Souslov, A. G. Abanov, and V. Vitelli, Odd viscosity in chiral active fluids, Nat. Commun. **8**, 1573 (2017).

[93] V. Soni, E. Bililign, S. Magkiriadou, S. Sacanna, D. Bartolo, M. J. Shelley, and W. T. M. Irvine, The free surface of a colloidal chiral fluid: Waves and instabilities from odd stress and Hall viscosity, arXiv:1812.09990.

[94] C. Scheibner, A. Souslov, D. Banerjee, P. Surowka, W. T. M. Irvine, and V. Vitelli, Odd elasticity, arXiv:1902.07760.